Terrestrial water mass load changes from Gravity Recovery and Climate Experiment (GRACE)

K.-W. Seo,[1,2] C. R. Wilson,[1] J. S. Famiglietti,[3] J. L. Chen,[4] and M. Rodell[5]

Received 13 May 2005; revised 20 January 2006; accepted 30 January 2006; published 16 May 2006.

[1] Recent studies show that data from the Gravity Recovery and Climate Experiment (GRACE) is promising for basin- to global-scale water cycle research. This study provides varied assessments of errors associated with GRACE water storage estimates. Thirteen monthly GRACE gravity solutions from August 2002 to December 2004 are examined, along with synthesized GRACE gravity fields for the same period that incorporate simulated errors. The synthetic GRACE fields are calculated using numerical climate models and GRACE internal error estimates. We consider the influence of measurement noise, spatial leakage error, and atmospheric and ocean dealiasing (AOD) model error as the major contributors to the error budget. Leakage error arises from the limited range of GRACE spherical harmonics not corrupted by noise. AOD model error is due to imperfect correction for atmosphere and ocean mass redistribution applied during GRACE processing. Four methods of forming water storage estimates from GRACE spherical harmonics (four different basin filters) are applied to both GRACE and synthetic data. Two basin filters use Gaussian smoothing, and the other two are dynamic basin filters which use knowledge of geographical locations where water storage variations are expected. Global maps of measurement noise, leakage error, and AOD model errors are estimated for each basin filter. Dynamic basin filters yield the smallest errors and highest signal-to-noise ratio. Within 12 selected basins, GRACE and synthetic data show similar amplitudes of water storage change. Using 53 river basins, covering most of Earth's land surface excluding Antarctica and Greenland, we document how error changes with basin size, latitude, and shape. Leakage error is most affected by basin size and latitude, and AOD model error is most dependent on basin latitude.

Citation: Seo, K.-W., C. R. Wilson, J. S. Famiglietti, J. L. Chen, and M. Rodell (2006), Terrestrial water mass load changes from Gravity Recovery and Climate Experiment (GRACE), *Water Resour. Res.*, *42*, W05417, doi:10.1029/2005WR004255.

1. Introduction

[2] The NASA/Deutsches Zentrum fur Luft und Raumfahrt (DLR) Gravity Recovery and Climate Experiment (GRACE) satellite mission was launched in March 2002. It consists of two identical satellites at about 500 km altitude, separated by about 220 km, in identical near-polar orbits. GRACE measures Earth's gravity field and its changes over time using range-rate perturbations between the two satellites sensed with a microwave interferometer. Each satellite is also tracked with an onboard GPS receiver. Perturbations due to nongravitational forces (such as atmospheric drag) are removed using an accelerometer mounted at the mass center of each satellite. GRACE detects spatial and temporal variations of Earth's gravity field with astonishing sensitivity. Published results have demonstrated that GRACE is able to detect changes in mass corresponding to surface water loads of 1 cm, with horizontal dimensions of hundreds of km and larger [*Wahr et al.*, 2004].

[3] Recent studies [e.g., *Chambers et al.*, 2004; *Tapley et al.*, 2004; *Wahr et al.*, 2004; *Ramillien et al.*, 2005; *Schmidt et al.*, 2006] show that GRACE can be used to estimate changes in terrestrial water storage at basin scales. Evapotranspiration, a critical but difficult to constrain component of the water cycle, can be estimated by combining GRACE and other observations [*Rodell et al.*, 2004b]. *Swenson et al.* [2003] estimated GRACE error over North American basins from simulated GRACE data, but error estimates were based on prelaunch satellite measurement error predictions, approximately 40 to 50 times smaller than current error levels [*Wahr et al.*, 2004]. In this study, we assess realistic GRACE errors globally and provide a comprehensive global comparison between climate model predictions and GRACE estimates.

[4] There are few direct observations to compare with GRACE products, so we must rely on indirect methods to quantify errors, using four resources: internal error measures reported with GRACE products; temporal (monthly) variations in GRACE spherical harmonic (SH) coefficients and related water storage estimates; independent water storage estimates from numerical models of land surface processes; and atmospheric and ocean model results used in GRACE processing and reported with GRACE data products. An

[1]Department of Geological Sciences, Jackson School of Geosciences, University of Texas at Austin, Austin, Texas, USA.
[2]Now at Jet Propulsion Laboratory, California Institute of Technology, Pasadena, California, USA.
[3]Department of Earth System Science, University of California, Irvine, California, USA.
[4]Center for Space Research, University of Texas at Austin, Austin, Texas, USA.
[5]NASA Goddard Space Flight Center, Greenbelt, Maryland, USA.

0043-1397/06/2005WR004255$09.00

Table 1. Summary of the Data

Type	Data
Monthly GRACE SH coefficients	GRACE data
GRACE internal error	GRACE measurement noise
Numerical models	synthetic GRACE data (GLDAS+ECCO+NCEP-AOD model)

additional complication is that there is no unique way to compute water storage changes from GRACE spherical harmonics. We use four different methods of combining harmonics, called basin filters, including one new method, described in section 2.2.

[5] Accuracy of water storage estimates from GRACE is limited by precision of the GRACE measurement system, which we estimate from internal error measures reported with GRACE products. We refer to this as measurement noise. A second error source is inaccuracies in atmospheric and ocean fields used to remove effects of ocean and atmosphere mass redistribution from GRACE observations. We refer to this as atmosphere-ocean dealiasing error (AOD). A third error source, leakage error, arises from a limited range of spherical harmonics used to represent gravity field variations. Leakage error is estimated from water storage fields taken from climate models by using the same finite range of SH coefficients available from GRACE. We examine these three error sources individually, and in combination, for river basins with diverse sizes, shapes, hydrologic regimes, and geographic locations.

2. Data and Methods

2.1. Data

2.1.1. GRACE Products and Internal Errors

[6] GRACE products and internal errors are available at PO.DAAC (http://podaac.jpl.nasa.gov/grace) and ISDC (http://isdc.gfz-potsdam.de/grace). Near-monthly (13–45 days) solutions are added as they are produced, beginning with April/May 2002. Here we use 13 solutions from August 2002 to December 2003. December 2002, January 2003, May 2003, and June 2003 results are not available. Separate bimonthly solutions for both April and May 2002 and April and May 2003 are not included in our analysis. Since most conclusions are based upon synthetic data constructed to resemble available GRACE fields, these omissions do not affect our results. GRACE products include SH degrees and orders up to 120. We omit coefficients beyond degrees 50 (spatial scales smaller than about 400km) and recognize that SH degrees larger than about 15 suffer from significant errors in current GRACE time-varying fields. Mean SH coefficients are computed from the series of 13 monthly SH coefficients and time variations are given with respect to these mean coefficients. Reported internal error (a standard deviation for each coefficient) is determined from the misfit of GRACE SH coefficients to measured data, and does not fully represent all error sources.

2.1.2. Numerical Models

[7] Redistribution of atmospheric and oceanic mass, and terrestrial water storage variations are the major contributors to temporal gravity changes at timescales of a few years and less. Atmospheric mass estimates are from NOAA's National Centers for Environmental Prediction (NCEP) analysis system [*Kalnay et al.*, 1996], ocean mass redistribution is taken from the multi-institutional Estimating the Circulation and Climate of the Ocean (ECCO) project [*Fukumori et al.*, 2000], and terrestrial water storage variations are from NASA's Global Land Data Assimilation System (GLDAS) driving the Noah land surface model with forcing from a combination of observations and atmospheric analyses [*Rodell et al.*, 2004a]. Mean fields from these models were computed for the 13 GRACE sample intervals over the period August 2002 to December 2003, and residual mass fields were fit to SH functions up to degree and order 50.

[8] In a dealiasing process, GRACE products have estimated effects of atmospheric and ocean mass redistribution removed. The European Center for Medium-Range Weather Forecasts (ECMWF) numerical model is used to remove atmospheric mass redistribution, and a barotropic model driven by surface winds and pressure is used to remove ocean redistribution. SH coefficients representing the sum of ECMWF and ocean model monthly mean fields are reported with GRACE data. Dealiasing is necessary because a sampling interval of one month is long compared with timescales of mass redistribution in the atmosphere and oceans. If dealiasing were perfect, the remaining time-variable signal in GRACE SH coefficients should be due to terrestrial water storage changes. Unfortunately, the AOD models are imperfect. The ocean model lacks baroclinic effects (associated with internal density changes), and has other deficiencies, for example, no Arctic Ocean. Atmospheric mass redistribution from ECMWF is similarly imperfect. For example, large errors in surface pressure fields are expected in regions of sparse data coverage.

2.1.3. Synthetic GRACE Data

[9] To generate synthetic GRACE data, we start with a SH representation of the sum of monthly mean GLDAS, ECCO, and NCEP fields, and subtract GRACE AOD fields for that month. We estimate AOD model error as the difference between GRACE AOD model fields and the

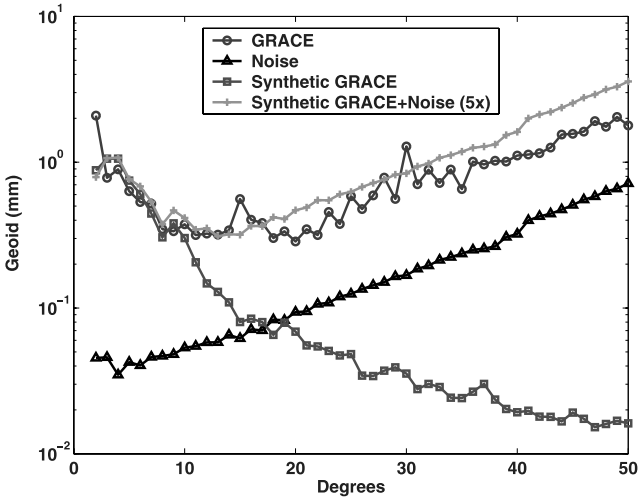

Figure 1. Spectra of GRACE data (circles), GRACE internal error (triangles), synthetic GRACE data (squares), and sum of synthetic GRACE data and the noise multiplied by 5 (crosses) for September 2002.

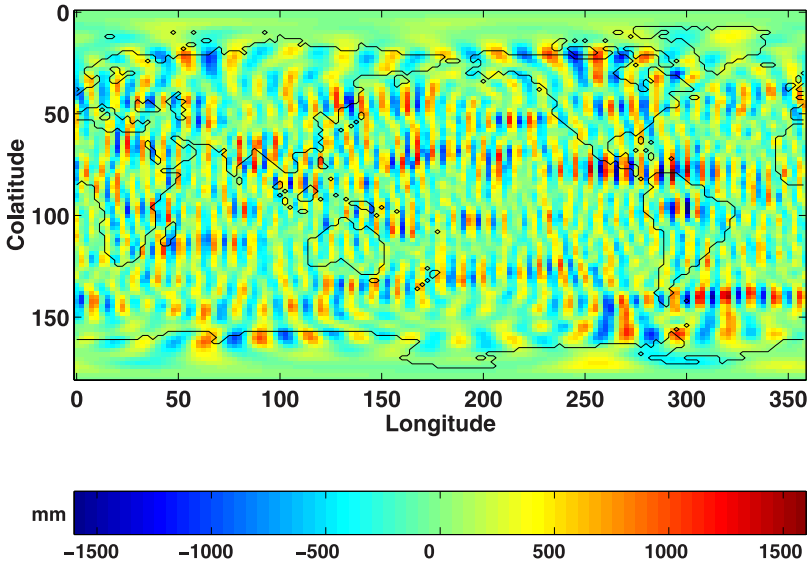

Figure 2. Surface load map from GRACE SH coefficients up to degrees and orders 50 for October 2003. The unit is mm water thickness.

sum of NCEP and ECCO fields. The result simulates gravity change seen by GRACE due to terrestrial water redistribution plus errors in AOD fields. AOD errors are approximated by the difference between NCEP and ECMWF and between ECCO and barotropic ocean models. The two sets of models are not entirely independent since they are driven by a similar set of observations, so the estimate of AOD model error is probably low. Real GRACE

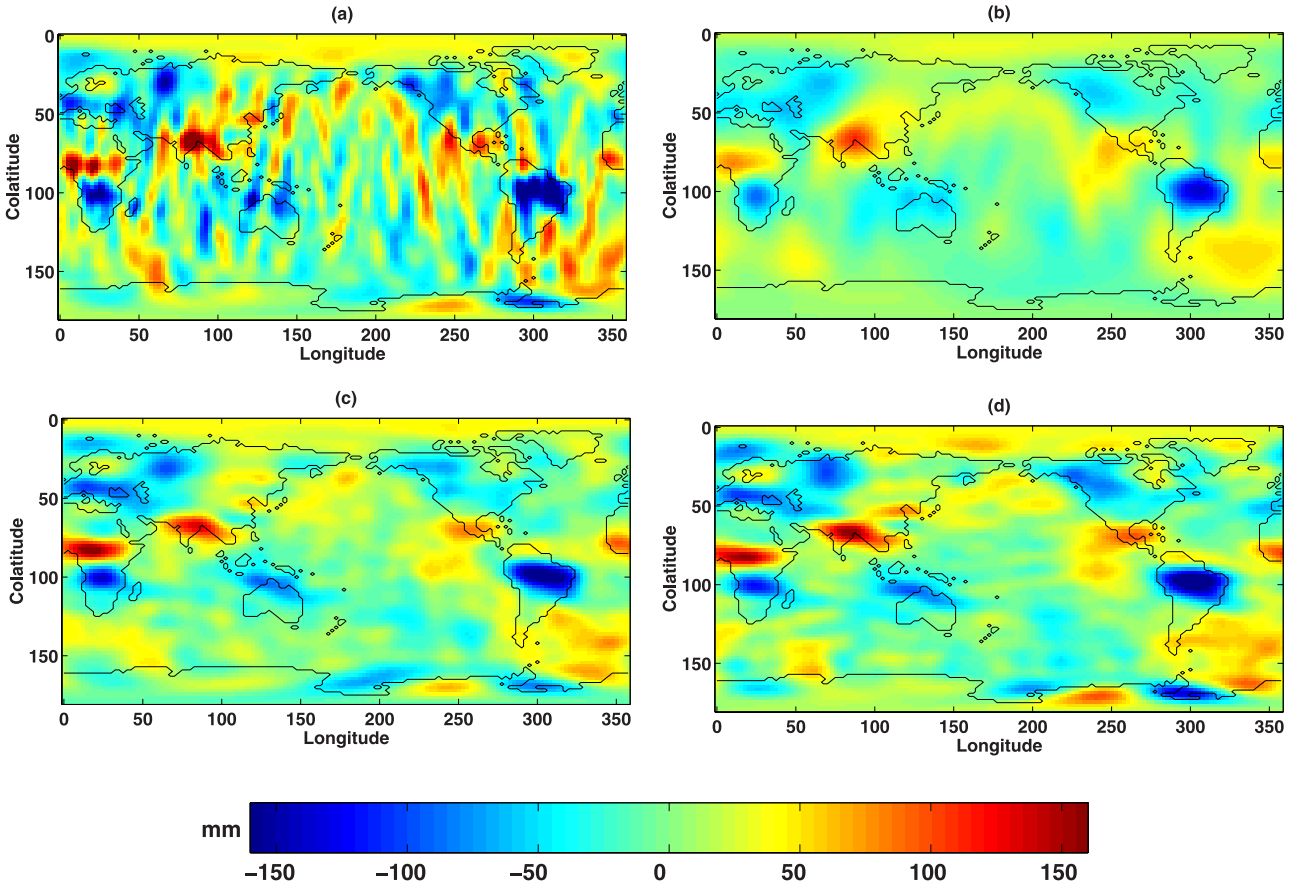

Figure 3. Surface load maps from GRACE SH coefficients using basin filters for October 2003: (a) 500 km Gaussian smoothing, (b) 1000 km Gaussian smoothing, (c) the dynamic filter using numerical models for signal variances, and (d) the dynamic filter using GRACE SH coefficients for signal variances. The units are mm water thickness.

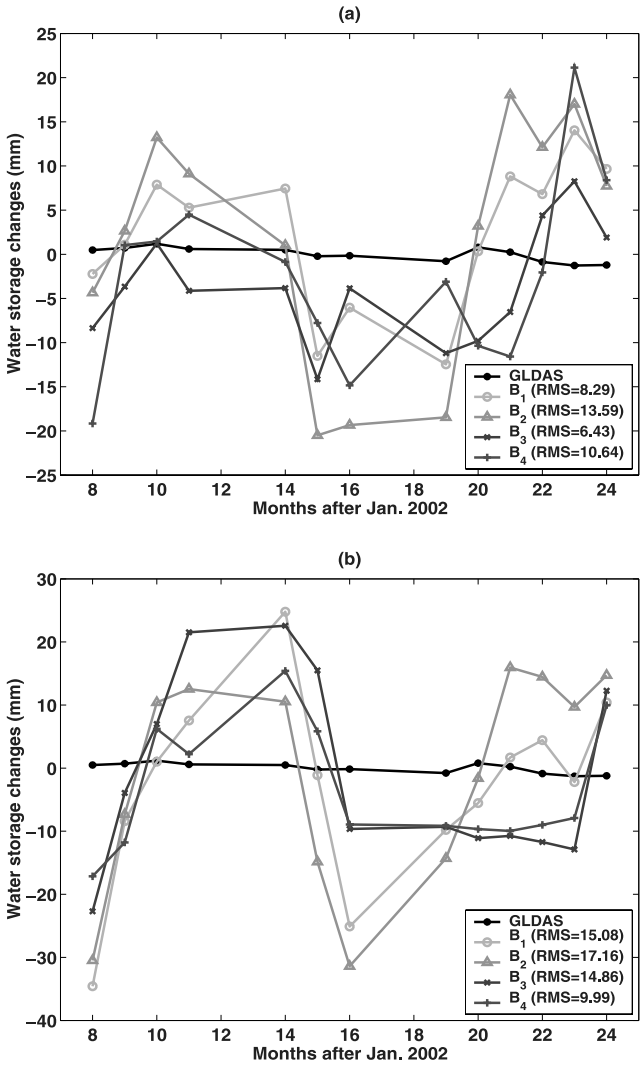

Figure 4. Water storage changes over the Sahara desert using B_1, B_2, B_3, and B_4 from (a) synthetic GRACE plus measurement noise and (b) GRACE.

data may have additional errors associated with the ocean tide model, measurement noise, and other effects, including aliasing. Table 1 summarizes the data used in this study.

[10] Figure 1 shows a graph of the logarithm of SH coefficient amplitude versus SH degree. This is analogous to a power spectrum in time series studies. In this case the horizontal axis, SH degree, corresponds to spatial frequency. The spatial scale (reciprocal of spatial frequency) associated with each degree is half the circumference of the Earth divided by SH degree. SH degree is equivalent to spatial frequency in a north-south direction, and at each SH degree, east-west spatial frequency is described by SH order ranging from 0 (constant over all longitudes) to degree number. Conventional practice is to combine coefficients from all orders at each degree to produce the spectrum, as in Figure 1. Figure 1 shows spectra for September 2002 GRACE SH coefficients and associated GRACE internal error. For the same month, Figure 1 shows also spectra of synthetic GRACE data, and synthetic GRACE data plus internal error magnified by a factor of 5. The internal error is scaled up to represent probable GRACE measurement noise levels.

[11] Figure 1 shows that spectra of GRACE and synthetic GRACE data agree well below about SH degree 10. Above degree 10, the spectra deviate, suggesting that errors become dominant with increasing SH degree. Adding internal error multiplied by 5 to synthetic data produces a synthetic spectrum that matches GRACE's fairly well. However, there are some obvious differences. One is that the GRACE SH degree 2 amplitude is much larger than the synthetic. *Chen et al.* [2004] suggest that degree 2 errors greatly exceed those described by the internal error spectrum, and degree 2 SH coefficients are not considered in our study. The other difference evident in Figure 1 is GRACE spectral peaks near SH degrees 15 and 30, absent in the synthetic spectra. These peaks are likely due to alias errors [*Seo and Wilson*, 2005b] which arise because the GRACE ground track does not sample the entire world simultaneously. The situation is familiar in time series analysis, where signal variations above the Nyquist frequency (half the sampling frequency) become aliased, appearing as other frequencies. In this case, the problem is more complex because sampling is in two spatial dimensions and in time.

2.2. Basin Filter Design

[12] Changes in surface loads (water storage with other signals removed) are estimated by forming a linear combination of GRACE SH coefficients in the following way [*Wahr et al.*, 1998]

$$\Delta\sigma(\phi,\lambda) = \frac{R\rho_E}{3}\sum_{l=0}^{N}\sum_{m=0}^{l}\tilde{P}_{lm}(\cos\phi)\frac{2l+1}{1+k_l} \cdot (C_{lm}\cos m\lambda + S_{lm}\sin m\lambda) \quad (1)$$

where $\Delta\sigma$ is water thickness, l and m are degree and order, $\tilde{P}_{lm}$ is the fully normalized Legendre functions, R, ρ_E, ϕ, and λ are mean Earth's radius, density, latitude, and longitude, and C_{lm} and S_{lm} are GRACE SH coefficients. k_l is the set of Love numbers to account for Earth deformation due to loading effects, and N, the maximum SH degree, is set to 50 in this study.

[13] Figure 2 shows a surface load map using (1) and GRACE data for October 2003 up to SH degree 50. North-south stripes dominate the map, and features related to water storage are obscured. Errors at high SH degree (above degree 10) dominate the picture, as evident in Figures 1 and 2. Basin filters, used to form the linear combination of SH coefficients, must be devised to suppress the influence of noisy high degree and order SH coefficients. Various strategies for designing basin filters have been proposed. For example, *Swenson and Wahr* [2002] and *Swenson et al.* [2003] developed optimum filters using estimates of signal variance and spatial correlation. Here we employ two types of filters. The first reduces SH amplitudes with increasing degree using a Gaussian weight. An adjustable parameter leaves an effective spatial resolution (r) in the resulting maps [*Swenson and Wahr*, 2002]. Figure 3a shows water storage maps from Gaussian filtered GRACE SH coefficients when r is 500 km. We call this basin filter B_1. Figure 3b shows the result for 1000 km resolution, filter B_2. 500 km resolution leaves some stripes, but 1000 km yields maps with clear water storage signals over Amazon,

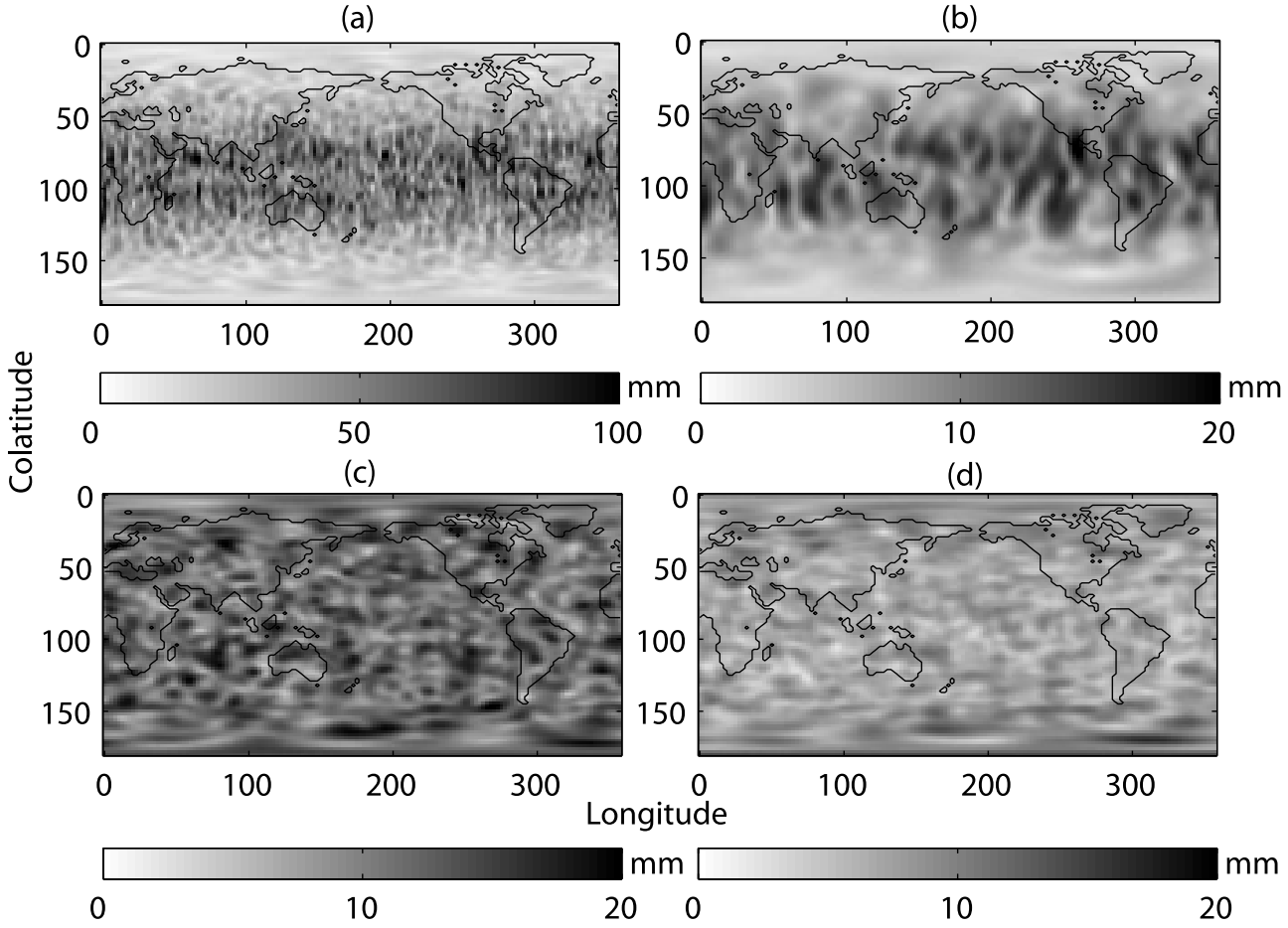

Figure 5. Estimation of RMS GRACE measurement noise from the four basin filters in mm water thickness. Noise estimations from (a) B_1, (b) B_2, (c) B_3, and (d) B_4.

Ganges, and Niger basins. Additional smoothing (Figure 3b) reduces the estimated signal amplitude relative to Figure 3a by about 25%. This implies a tradeoff between suppression of noise and accuracy of the estimate. Without further information a criterion for selecting an optimum r is not obvious. In addition, Gaussian smoothing tends to produce water storage maps with rounded contours, deviating from true basin shape. This is because Gaussian smoothing corresponds to spatial convolution with a circularly symmetric function.

[14] The second filter type, called a dynamic filter, performs smoothing in a more complex way. It uses GRACE error estimates and GLDAS and ECCO model fields, or GRACE data itself, to compute weights for each coefficient. Relative to Gaussian smoothing, it applies filter weights that vary with both SH degree and order. Filter weights may change each month as signal and noise changes, hence the name dynamic. When the numerical model estimates are good, this idea works well [*Seo and Wilson*, 2005a]. The dynamic filter scales each SH coefficient by the ratio of signal variance divided by signal plus noise variance. This is a least squares optimum approach. Figure 3c shows the result with the dynamic filter using GLDAS to estimate signal and 5 times GRACE internal error as the noise estimate. We call this filter B_3. Signal variances are from numerical model fields for each month. Figure 3c shows that water storage signals associated with river basins are less rounded in contour than those in Figure 3b, because weights can vary with SH degree and order. The equivalent spatial convolution is not isotropic.

[15] The success of the dynamic filter depends on the accuracy of the numerical models used as signal estimates. GLDAS and ECCO do not cover high latitudes, and have other deficiencies. An alternative is to use GRACE SH coefficients themselves as an estimate of signal in the dynamic filter. We call this filter B_4. We remove alias error peaks at degrees 15 and 30 (Figure 1) before using GRACE coefficients to form dynamic filter weights. We scale GRACE SH coefficients by internal error in Figure 1 normalized by the minimum value, to estimate signal variance for B_4. Figure 3d is the dynamic filter water storage map using GRACE SH coefficients. Amplitudes are similar to those in Figure 3c, but generally larger at high latitudes. This difference is likely a consequence of small signal amplitudes in GLDAS and ECCO at high latitudes. GRACE observations are probably best at high latitudes due to frequent sampling associated with the polar orbit. Figures 3c and 3d show the east-west elongated features in dynamic filter estimates. This is because the dynamic filter tends to suppress high-order SH coefficients at any particular SH degree, in response to GRACE internal error values which increase with SH order [*Han et al.*, 2005].

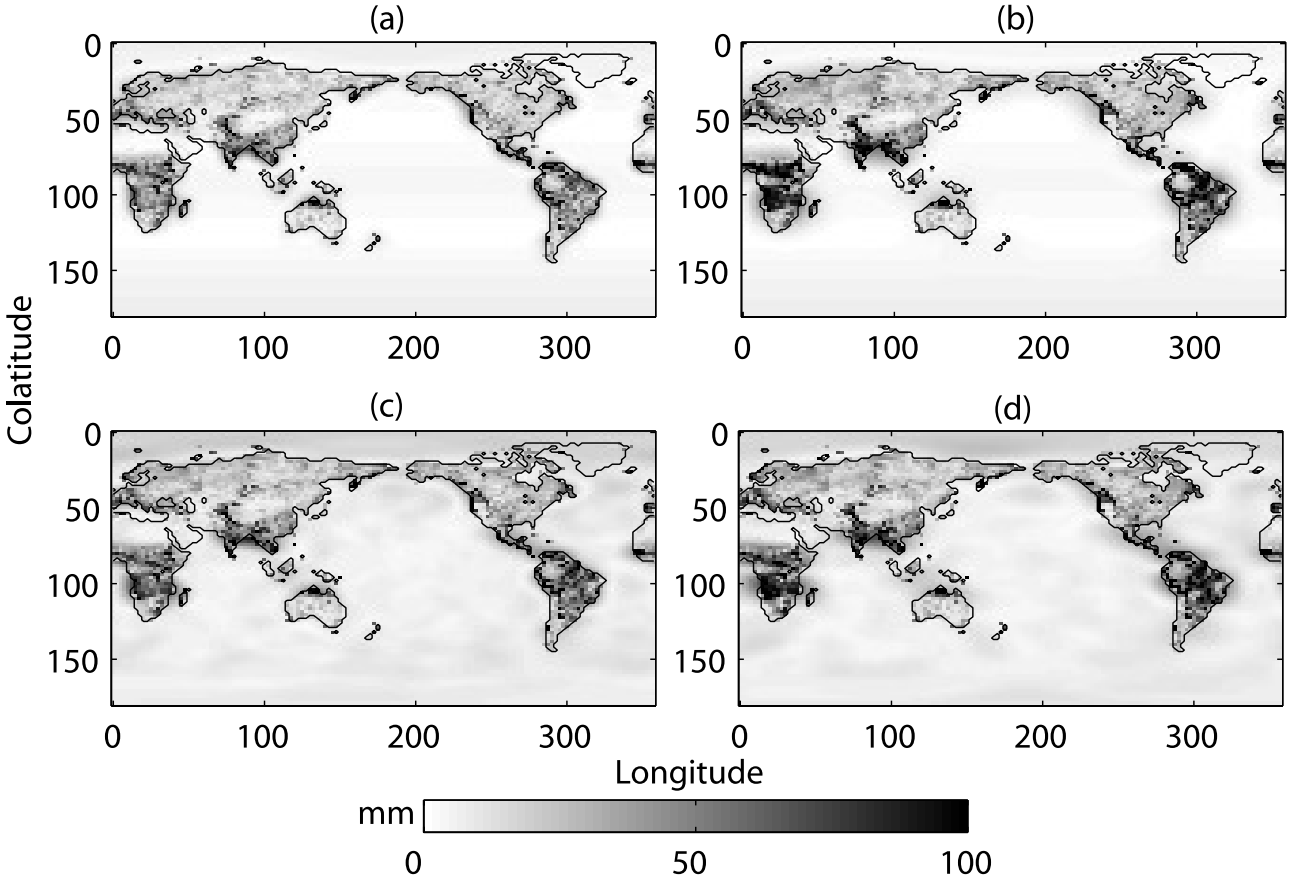

Figure 6. RMS leakage error from the four basin filters in mm water thickness. Error estimations from (a) B_1, (b) B_2, (c) B_3, and (d) B_4.

This causes zonal (east-west) SH terms to be more evident in the water storage estimates, as seen in Figures 3c and 3d.

2.3. Assessment of Basin Filters

[16] Over the Sahara desert, the signal level due to water storage is essentially zero. Therefore the desert should be a good target to assess the four basin filters. Figure 4a shows time series of water storage change over the Sahara from synthetic data plus Gaussian random numbers to simulate measurement noise for the four basin filters. Figure 4b shows similar time series using GRACE data. The results in Figures 4a and 4b are similar, showing strong seasonal fluctuations. GLDAS predictions are close to zero, as expected.

[17] Apparent seasonal variations in Figure 4 are almost certainly AOD model and leakage error. For example, in the time series from B_2 of Figure 4a, RMS measurement noise, leakage error and AOD model error are 4.97, 7.46 and 8.01 mm water thickness respectively. Leakage is probably from regions to the south where water storage changes are large. RMS values of time series provide reasonable estimates of errors. For synthetic data (Figure 4a), B_3 performs best, while for GRACE data (Figure 4b), B_4 is best. This is not surprising since B_3 and B_4 are each designed to minimize leakage based on their respective data sets (GLDAS for B_3 and GRACE for B_4). This verifies that the dynamic filter strategy is effective in minimizing leakage. This also implies that the basin filter for GRACE data which minimizes leakage is probably B_4.

3. Results

3.1. Error Evaluation for Basin Filters

[18] Using synthetic GRACE data the correct answer is known, and errors associated each filter can be separated into contributions from measurement noise (E_1), leakage [*Seo and Wilson*, 2005a] (E_2), and AOD model errors (E_3). These three errors can be computed for an individual river basin, or represented in map form for the globe. Leakage errors include both the smoothing from a finite range of SH degrees, and accompanying contamination of estimates from load changes in nearby regions. Aliasing error is absent in synthetic data. Error estimates represent RMS values for 13 months of synthetic data.

[19] Measurement noise is simulated using normally distributed random numbers with standard deviations equal to GRACE internal error multiplied by 5. Figure 5 shows this noise after filtering by B_1 through B_4. Figure 5a shows that B_1 noise is strongest at low latitudes. This is due to the sparse low latitude sampling properties of the GRACE polar orbit. B_2 filtered noise, Figure 5b, shows a similar effect, but reduced in amplitude. Both show longitudinal stripes that remain because measurement noise increases at high SH order, due to the sampling properties of the polar orbit. B_3

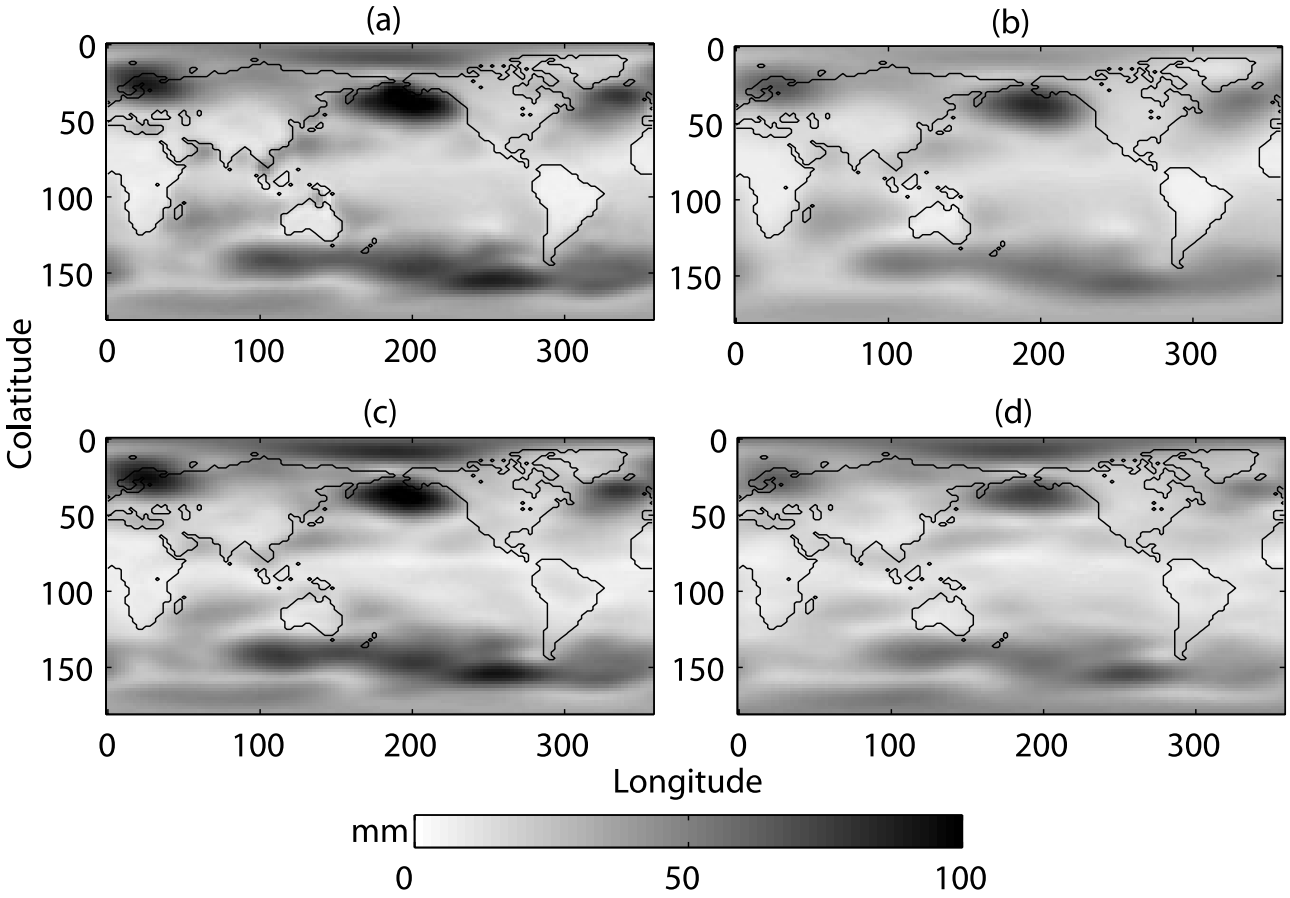

Figure 7. RMS AOD model error from the four basin filter in mm water thickness. Error estimations from (a) B_1, (b) B_2, (c) B_3, and (d) B_4.

filtered noise is shown in Figure 5c. The sum of E_1 and E_2 variance is minimized in this case. B_3 filtered noise lacks the longitudinal stripes of Figures 5a and 5b, because it suppresses noisy high-order terms. B_4 filtered noise (Figure 5d) shows the least noise among the four filters. The main conclusion from Figure 5 is that the basin filter has a first-order effect on contamination due to measurement noise. B_3 or B_4 appear most effective at minimizing this, leaving a spatial distribution of noise that appears random. This is a desirable property, since the noise would tend to average to zero over a large enough region. Gaussian smoothing can reduce the noise a comparable amount, but leaves longitudinal stripes, which may not average to zero when forming a regional average.

[20] Leakage error E_2 is the difference between gridded GLDAS output and GLDAS fields converted to SH form, then filtered with one of the four filters. Leakage error increases as high degree SH coefficients are suppressed to reduce measurement noise. Figure 6 shows the results. Comparing Figure 6a with 6b, E_2 is lower in Figure 6a because B_1 (500 km resolution) includes higher SH coefficients. Both Figures 6a and 6b show that leakage is concentrated in regions of high water storage variability, especially at low latitudes. B_3 leakage errors are similar to B_1, though somewhat larger in regions of high variability. B_4 (Figure 6d) shows greater leakage than Figure 5c, because B_4 coefficients are derived from GRACE, rather than true (GLDAS) signal.

[21] AOD model error E_3 is the difference between gravity changes from oceans plus atmosphere and predictions of the GRACE AOD models. We estimate this as the difference between [ECCO + NCEP] and the GRACE AOD model. This is probably a conservative error estimate since ECCO, NCEP, and GRACE AOD models incorporate common observational data sets. Figure 7 shows RMS AOD model error for the four basin filters. Significant error in some high-latitude regions may be due to sparse coverage of meteorological stations. The map also shows differences in northern Europe where station coverage is dense. This curious difference seems to be associated with a few large differences for particular months. AOD model error is not fully described by Figure 7 because it properly also includes alias error, not examined in this study.

[22] At each grid point we can estimate the RMS signal-to-noise ratio, by

$$\mathrm{SNR} = \frac{\mathrm{RMS}(T)}{\sqrt{\mathrm{RMS}(E_1)^2 + \mathrm{RMS}(E_2)^2 + \mathrm{RMS}(E_3)^2}} \qquad (2)$$

in which T is the GLDAS time series for that grid point. Comparing SNR maps in Figure 8, B_3 shows the highest SNR. This is not surprising, since B_3 is designed to maximize this quantity. B_4 (Figure 8d) shows a similar spatial pattern as in Figure 8c, but maximum SNR values are smaller. These maps define geographical locations

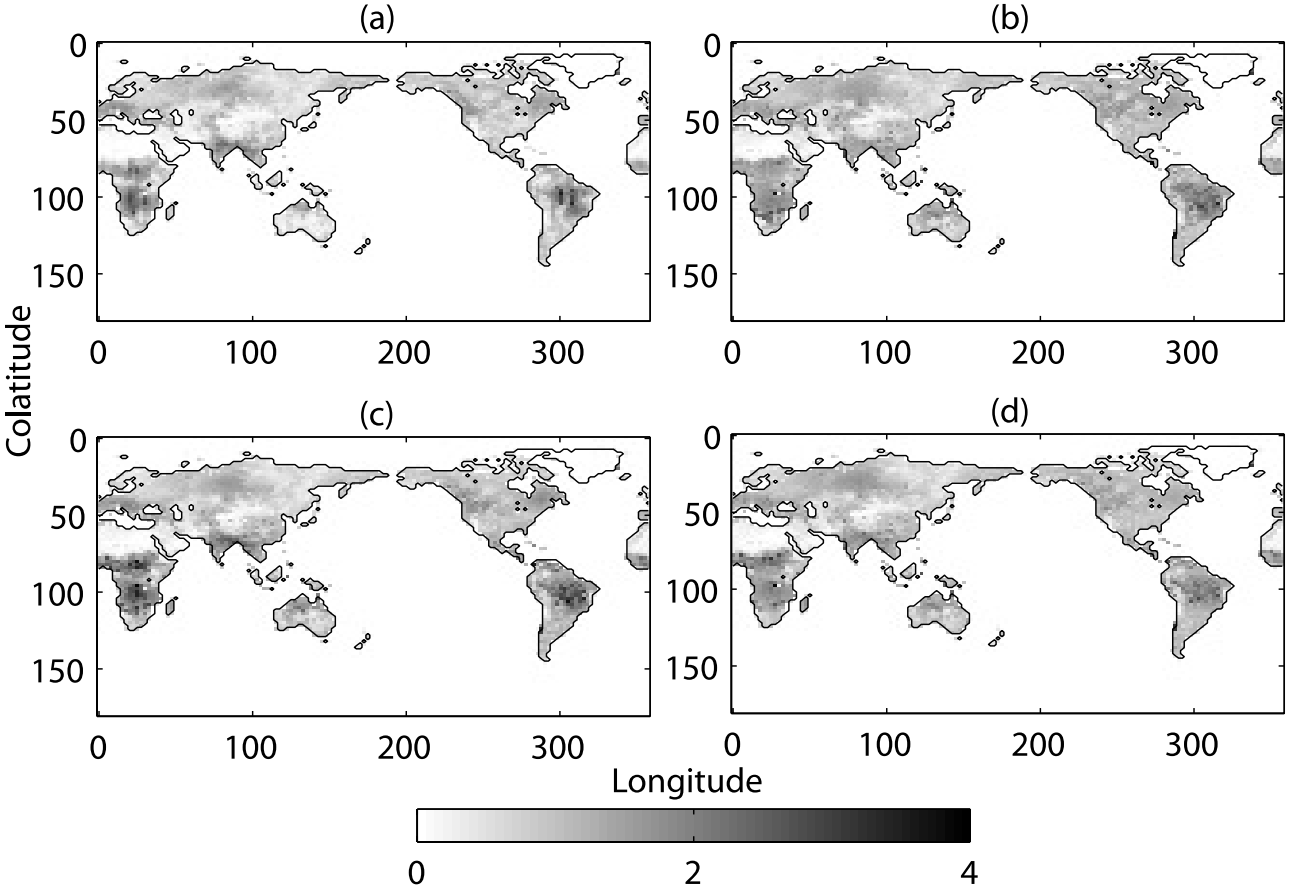

Figure 8. Signal-to-noise ratio from the four basin filters. Error estimations from (a) B_1, (b) B_2, (c) B_3, and (d) B_4.

where GRACE estimates should be useful in water storage studies, generally regions where SNR > 1. This excludes regions with arid climates, such as North Africa, central and east Asia, and others. The intertropical convergence zone shows the largest SNR.

3.2. Water Storage Variations for Selected Basins

[23] Twelve river basins are listed in Table 2 [*Graham et al.*, 1999]. Figure 9 shows geographic locations of the basins. These basins represent a variety of sizes and climate conditions. Water storage changes are recovered from the 13 monthly GRACE solutions, and associated errors are estimated from synthetic data plus measurement noise. Figure 10 shows time series from GRACE for each basin using the four basin filters. Water storage changes from GRACE show clear seasonal fluctuations, and are similar to GLDAS estimates. For small basins (Victoria, Mekong, Volta and Don), B_1 shows the greatest differences relative to the other three filters. This is because B_1 does not reduce the measurement noise efficiently in small basin. For the Orinoco basin, B_2 shows approximately half the amplitude of the other three filters. The smaller amplitude can be explained by the leakage error from the Amazon basin in which the seasonal phase is opposite to the Orinoco. These results confirm again that Gaussian smoothing is not an optimized method.

Table 2. Twelve River Basins

Map Number	River Basin	Size, km^2
1	Amazon (Brzail)	6,123,000
2	Congo (Zaire)	4,449,000
3	Mississippi (USA)	3,539,000
4	Yenisei (Russia)	2,398,000
5	Ganges (Bangladesh)	1,926,000
6	Orinoco (Venezuela)	1,257,000
7	Yukon (USA)	953,000
8	Danube (Romania)	841,000
9	Victoria (Australia)	812,000
10	Mekong (Vietnam)	745,000
11	Volta (Ghana)	573,000
12	Don (Russia)	280,000

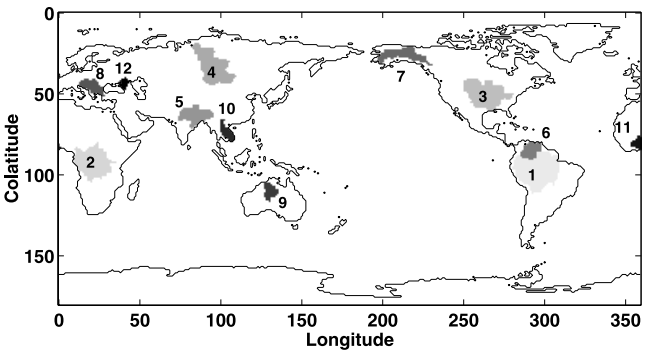

Figure 9. Twelve river basins.

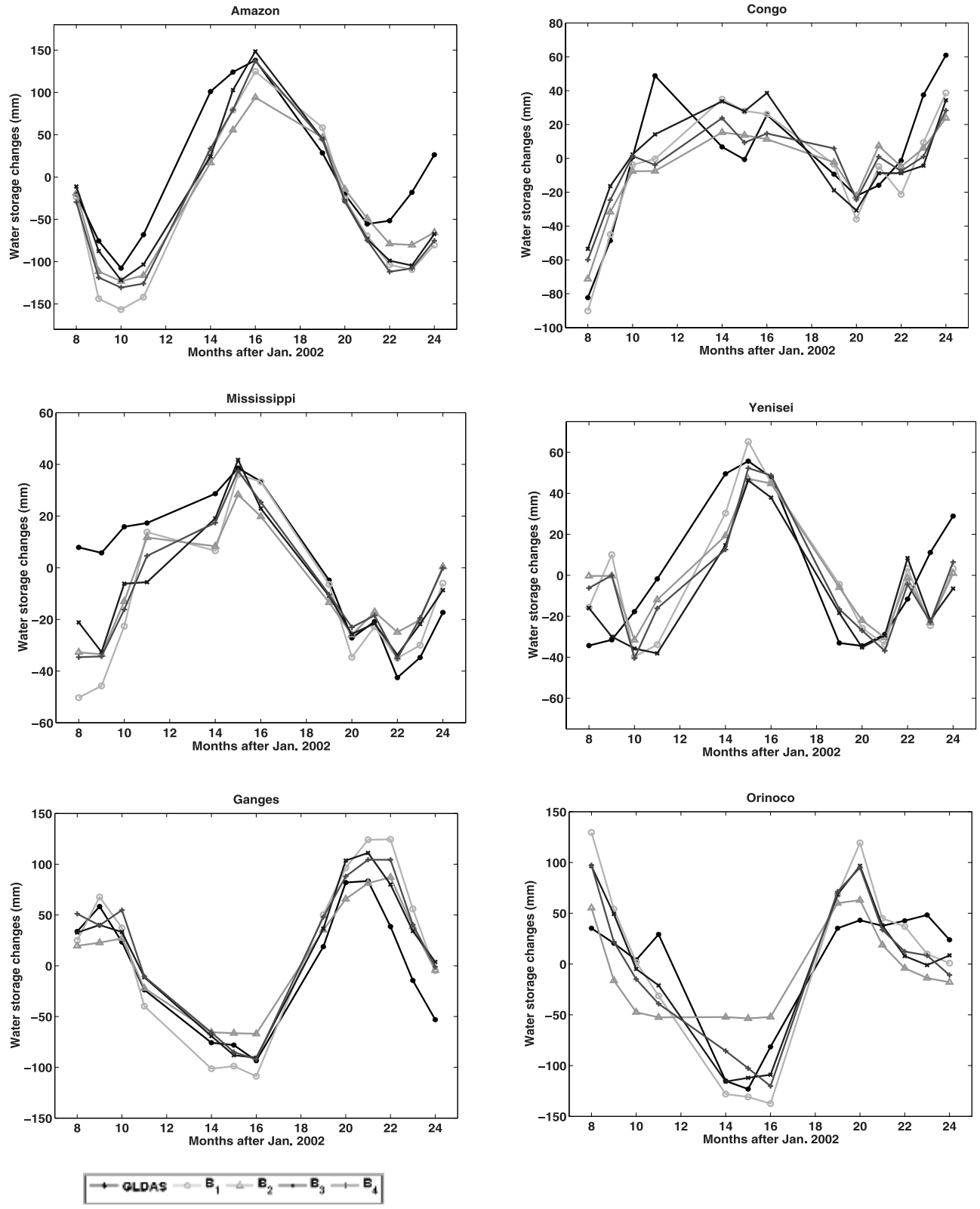

Figure 10. Water storage changes from GLDAS and GRACE.

[24] Figure 11a shows best fit annual sinusoid RMS values for the time series in Figure 10. Basin numbers are given in Table 2. Results for B_1, B_2, B_3, and B_4, are identified using separate colors. The three panels use mm of water equivalent, and are offset from one another vertically by 100 mm for clarity. The bottom panel shows RMS GRACE errors. Errors due to the sum of measurement noise, leakage, and AOD model error are shown as

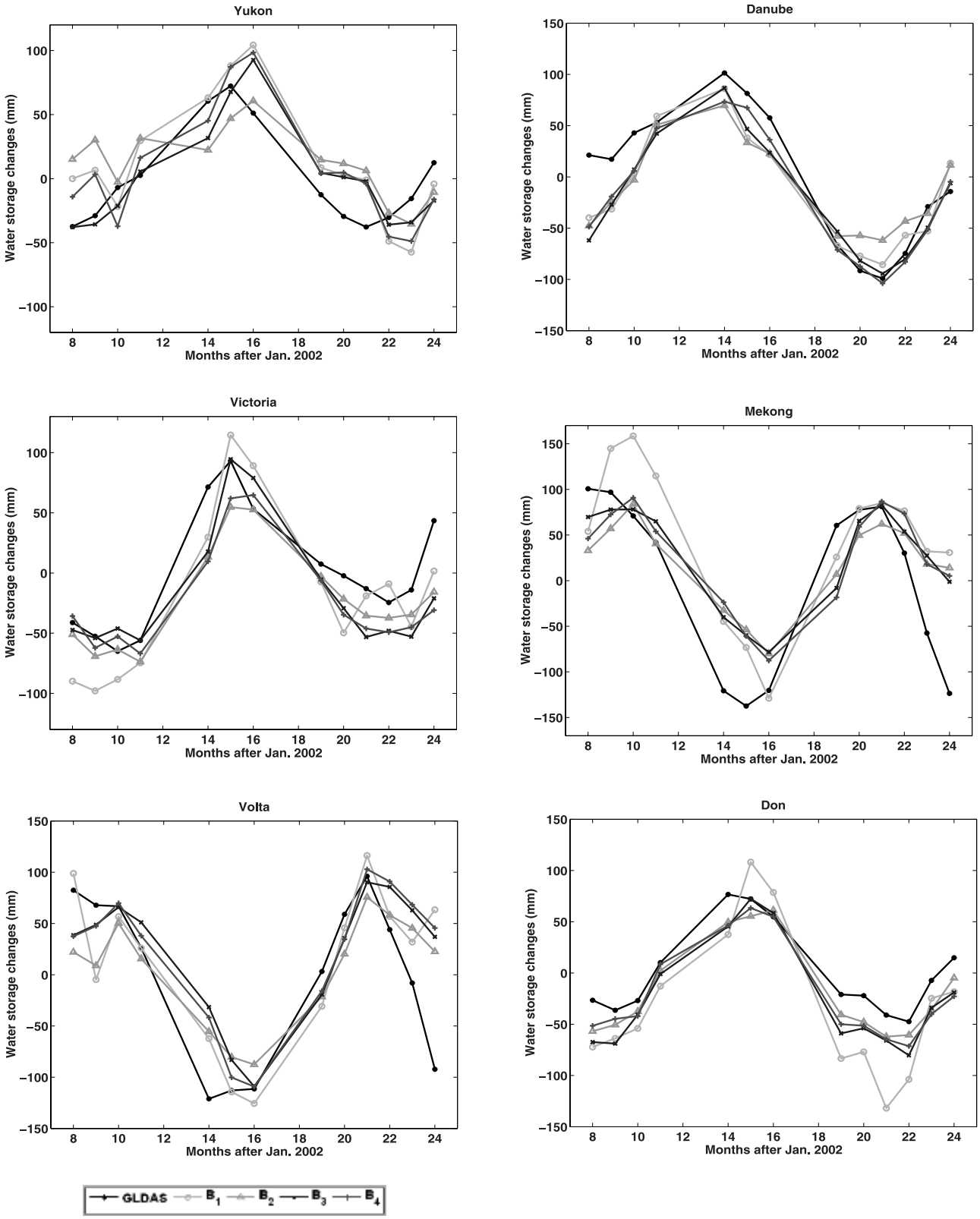

Figure 10. (continued)

a single point. Errors are estimated from synthetic GRACE data and GRACE measurement noise. The middle panel shows RMS estimates for synthetic GRACE data plus measurement noise, and GLDAS without filtering. The top panel shows RMS values of GRACE data. Figure 11b is similar to Figure 11a, showing RMS residuals relative to the best fit annual sinusoid.

[25] All basin filters produce similar RMS values for a given basin, and agree well with GLDAS, both for annual (Figure 11a) and nonannual components (Figure 11b). In

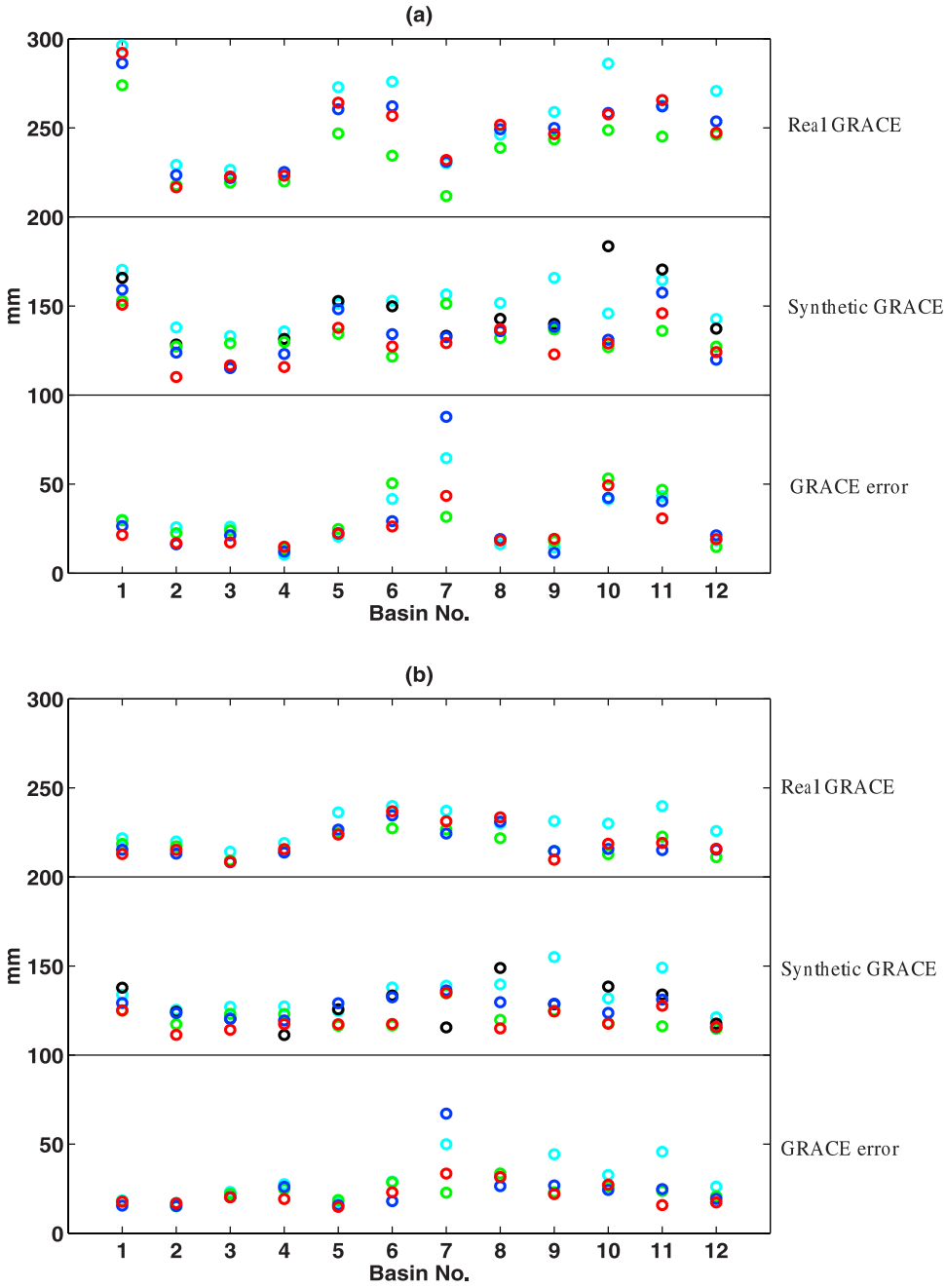

Figure 11. RMS values of GRACE error (bottom panels), synthetic GRACE signal plus measurement noise (middle panels), and real GRACE signal (top panels) over 12 basins. Cyan, green, blue, and red represent B_1, B_2, B_3, and B_4. Black circles in middle panels are GLDAS output without filtering. (a) RMS best fit annual amplitudes and (b) residuals relative to the best fit annual sinusoid.

general, annual RMS values from GRACE are higher than those of synthetic data. B_2 is predicted to produce the largest errors for annual amplitudes because, with 1000 km smoothing, it introduces significant leakage errors. B_1 errors are largest for nonannual residuals because B_1, with 500 km smoothing, retains noisy high-degree terms. Dynamic filters (B_3 and B_4) produce smaller errors for both annual and nonannual components.

[26] Figure 11a (bottom) indicates that Orinoco (6), Yukon (7), Mekong (10), and Volta (11) basins have large estimated annual errors. The cause is likely a combination of leakage and AOD model errors. Orinoco, Volta, and Mekong basins are adjacent to the Amazon, Sahara and the Pacific Ocean, respectively, with very different hydrological regimes. For example, Amazon and Orinoco water storage cycles are nearly of opposite phase, as in Figure 10, while the Sahara has virtually zero storage change. Both situations would lead to leakage errors. AOD model errors are suspected to be a problem for the Yukon as predicted in Figure 6.

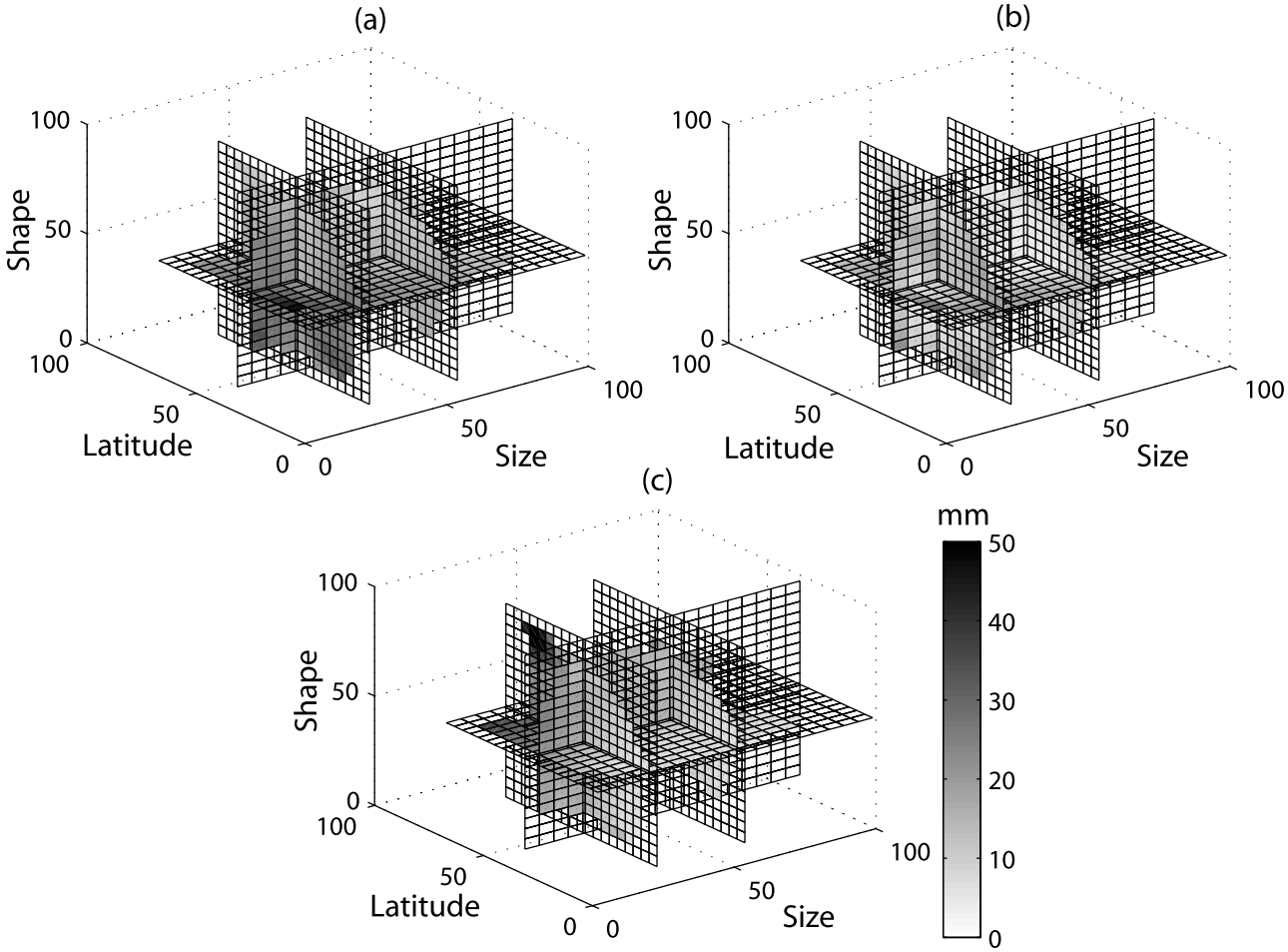

Figure 12. GRACE RMS error distribution filtered by B_1 with respect to basin size, latitude, and shape. (a) Measurement noise (E_1), (b) leakage error (E_2), and (c) AOD model error (E_3). The basin size, latitude, and shape are normalized. The detail description of the normalizations are described in section 5.

[27] We estimated RMS GRACE errors from synthetic data and measurement noise for 53 river basins, including the 12 above. This includes most of Earth's land surface, excluding Antarctica and Greenland. RMS error for each basin is the sum of annual and nonannual residual errors, for the 12 basins summarized in Figures 11a and 11b (bottom), plus values for the 41 additional basins. Basin size, latitude, and shape are used as independent variables in Figures 12 and 13 as a way of quantifying their effect on errors in water storage estimates. Basin size (area) is normalized relative to a maximum of 100, with the Amazon, being the largest with an area of 6,123,000 square km. Absolute value of latitude is used and ranges between 0 and 90. Basin shape is the normalized ratio of east-west and north-south dimensions computed by

$$\left[\frac{A-B}{\sqrt{A^2+B^2}}+1\right]\times 50 \tag{3}$$

in which A and B are longitudinal and latitudinal distances at basin center. Figure 12 shows measurement noise, leakage error, and AOD model error filtered by B_1. Figure 12a shows that low latitude, small size, and north-south elongated basins are associated with increased measurement noise. Measurement noise dependence on latitude is shown in Figure 4a. Because measurement noise is random, larger spatial averaging leads to smaller measurement noise. The longitudinal stripes in Figure 4a imply that a basin elongated in a north-south direction will be relatively more troubled by measurement noise. Figure 12b shows how leakage error is affected by basin size and latitude. However, with the 500 km smoothing of B_1, leakage error is relatively small, and there is little dependence. Figure 12c shows AOD error, varying with latitude as suggested by Figure 6a. Figure 13 shows similar results for B_3. Measurement noise is reduced considerably relative to Figure 12. Patterns of leakage and AOD model errors are similar to those in Figure 12. The dependence of leakage error on latitude is more obvious than in Figure 12.

[28] Using the 53 basin errors summarized in Figures 12 and 13, we fit linear functions by least squares to describe RMS measurement noise, leakage error, and AOD model error as a function of basin size (x), latitude (y), and shape (z). Table 3 shows coefficients for the estimated polynomials associated with B_1 and B_3. Residuals of GRACE errors for the 53 basins relative to the polynomial fit are shown in Figure 14. Circles are RMS GRACE errors, and

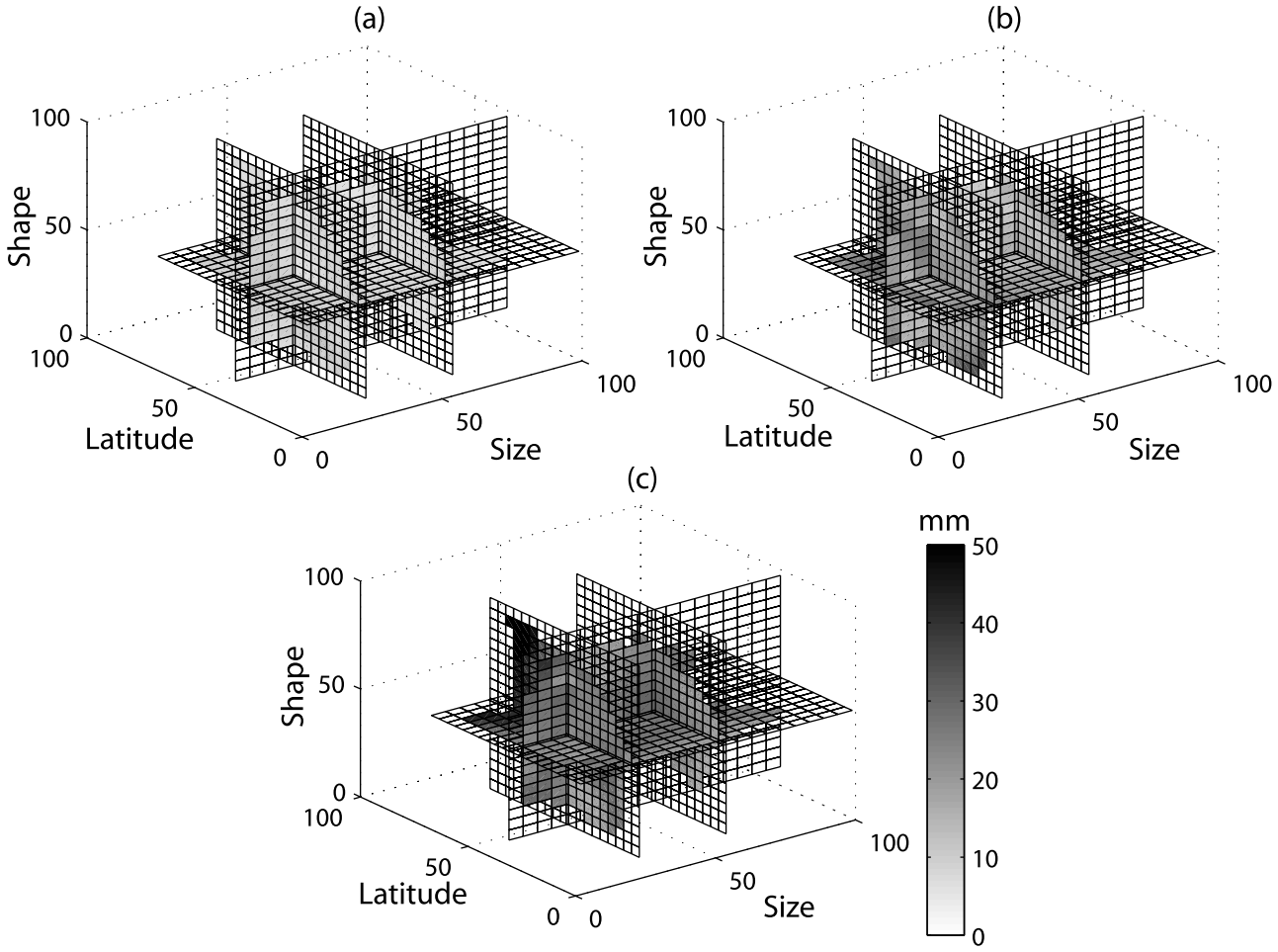

Figure 13. GRACE RMS error distribution filtered by B_3 with respect to basin size, latitude, and shape. (a) Measurement noise (E_1), (b) leakage error (E_2), and (c) AOD model error (E_3). The basin size, latitude, and shape are normalized. The detail description of the normalizations are described in section 5.

crosses are residuals. The polynomials do a good job of describing error dependence on size, latitude, and shape.

4. Conclusions

[29] With synthetic GRACE data, we examined Gaussian smoothing and dynamic filters. Gaussian smoothing (B_1 and B_2) applies the same weight to all SH orders at each SH degree, producing rounded water storage features. There are trade-offs in choosing the amount of Gaussian smoothing, with additional smoothing reducing signal amplitude. An objective criterion for choosing the amount of smoothing is not clear. Dynamic filters (B_3 and B_4) use a least squares criterion to filter each degree and order differently according to signal and error spectra. Dynamic filter coefficients can be fixed, or changed over time as the error and signal change. To implement the dynamic filters one requires additional information about signal strength, which can be obtained either from numerical models like GLDAS, or from GRACE product themselves. The dynamic filters force variance to be concentrated in regions where there are water storage variations. The dynamic filter concept was superior to Gaussian filtering in all the examples we examined.

[30] Global signal-to-noise ratio maps from the four basin filters are a guide to regions where currently released GRACE products can be useful in water storage studies. In general these are areas where SNR is greater than unity. This excludes many arid regions, but includes a fairly large fraction of the land surface. Water storage changes and associated errors are estimated over 12 basins and compared with GLDAS. For these large basins, the four basin filters perform similarly. When the goal is to produce a gridded water storage map, then spatial resolution is of paramount importance, and dynamic filters (B_3 or B_4) are preferred.

[31] Annual amplitudes for the 12 basins are larger for GRACE than synthetic data (from GLDAS), but nonannual residuals are about the same size. There may be multiple explanations. One is simply that GLDAS underestimates the

Table 3. Coefficients of Linear Polynomials Representing GRACE Errors[a]

	1	x	y	z
Noise (B_1)	45.2888	−0.3586	−0.3275	−0.0855
Leakage (B_1)	30.4823	−0.2819	−0.2018	−0.0526
AOD (B_1)	25.2369	−0.1278	0.2213	0.1299
Noise (B_3)	10.5450	−0.0571	−0.0076	−0.0098
Leakage (B_3)	37.0218	−0.2755	−0.1381	−0.0795
AOD (B_3)	11.6251	−0.1924	0.5037	0.1686

[a]Here x, y, and z are normalized variables for basin size, latitude, and shape, respectively. The detailed descriptions of the normalizations are described in section 5.

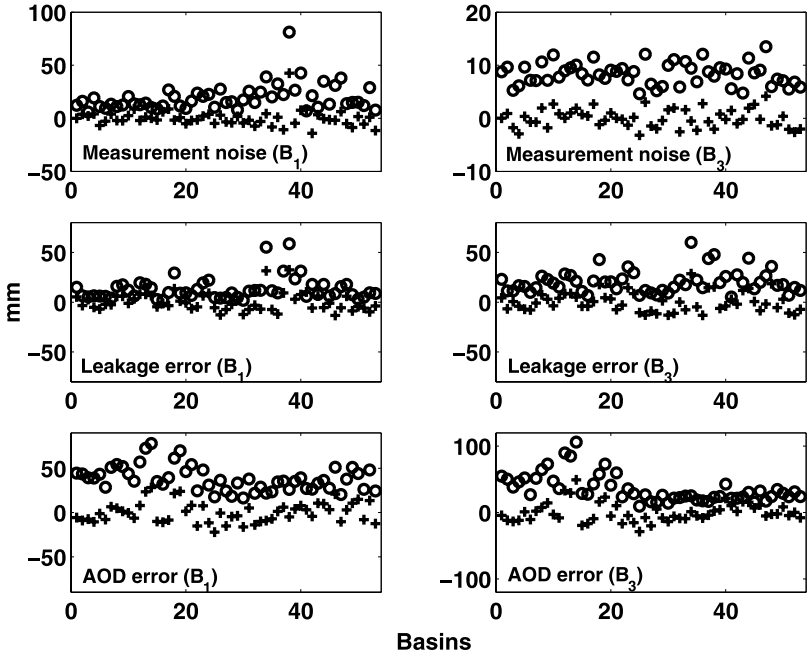

Figure 14. Circles are GRACE RMS errors for water storage change over basins by B_1 and B_3. Crosses are residuals relative to the polynomials, whose coefficients are listed in Table 2.

annual cycle in these basins, but interannual variations are more nearly correct. GLDAS does not include groundwater, a possibly significant element of annual storage changes. The GRACE annual cycle may also be larger than GLDAS because aliasing may contaminate the annual signal more than smaller nonannual residuals of random phase throughout the world. GRACE may also contain annual noise of unknown origin.

[32] For both annual and nonannual components, GRACE variations are less dependent on basin filters than those for synthetic data. This is evident in the smaller vertical scatter in the symbols of Figure 11. We suspect that true GRACE measurement noise is smaller than the noise model used to create synthetic data. This is suggested by Figure 1.

[33] Using 53 basins, we estimate measurement, leakage, and AOD model errors, and graph their dependence on basin size, latitude, and shape. These are the main variables anticipated to be important for a given basin. Linear polynomials fit by least squares provide an algorithm for predicting the likely errors for any basin. These polynomials summarize the error situation in current GRACE products. Future releases of GRACE products will likely have smaller errors, and the polynomials and other measures of error will certainly change. However, the general method, and other error descriptions such as the SNR map, are likely to be useful tools in the future.

[34] **Acknowledgments.** We thank Michiaki Sugita and three reviewers for their helpful comments and suggestions. This research was funded by NASA grants NAG5-8798, NGT5-30447, and NNG04GF22G. Additional support was provided by the Geology Foundation of the University of Texas.

References

Chambers, D. P., J. Wahr, and R. S. Nerem (2004), Preliminary observations of global ocean mass variations with GRACE, *Geophys. Res. Lett.*, *31*, L13310, doi:10.1029/2004GL020461.

Chen, J. L., C. R. Wilson, B. D. Tapley, and J. C. Ries (2004), Low degree gravitational changes from GRACE: Validation and interpretation, *Geophys. Res. Lett.*, *31*, L22607, doi:10.1029/2004GL021670.

Fukumori, I., T. Lee, D. Menemenlis, L. I. Fu, B. Cheng, B. Tang, Z. Xing, and R. Giering (2000), A dual assimilation system for satellite altimetry, paper presented at Joint TOPEX/Poseidon and Jason-1 Science Working Team Meeting, Univ. Corp. for Atmos. Res., Miami Beach, Fla.

Graham, S. T., J. S. Famiglietti, and D. R. Maidment (1999), 5-minute, 1/2-degree, and 1-degree data sets of continental watersheds and river networks for use in regional and global hydrologic and climate system modeling studies, *Water Resour. Res.*, *35*(2), 583–587.

Han, S.-C., C. K. Shum, C. Jekeli, C.-Y. Kuo, C. R. Wilson, and K.-W. Seo (2005), Non-isotropic filtering of GRACE temporal gravity for geophysical signal enhancement, *Geophys. J. Int.*, *163*, 18–25.

Kalnay, E., et al. (1996), The NCEP/NCAR 40-year reanalysis project, *Bull. Am. Meteorol. Soc.*, *83*, 1631–1648.

Ramillien, G., F. Frappart, and A. Cazenave (2005), Time variations of land water storage from an inversion of 2 years of GRACE geoids, *Earth Planet. Sci. Lett.*, *235*, 283–301.

Rodell, M., et al. (2004a), The Global Land Data Assimilation System, *Bull. Am. Meteorol. Soc.*, 381–394, doi:10.1175/BAMS-85-3-381.

Rodell, M., J. S. Famiglietti, J. L. Chen, S. I. Seneviratne, P. Viterbo, S. Holl, and C. R. Wilson (2004b), Basin scale estimates of evapotranspiration using GRACE and other observations, *Geophys. Res. Lett.*, *31*, L20504, doi:10.1029/2004GL020873.

Schmidt, R., et al. (2006), GRACE observations of changes in continental water storage, *Global Planet. Change*, *50*, 112–126, doi:10.1016/j.gloplacha.2004.11.018.

Seo, K.-W., and C. R. Wilson (2005a), Simulated estimation of hydrological loads from GRACE, *J. Geod.*, *78*, 442–456.

Seo, K.-W., and C. R. Wilson (2005b), Estimating GRACE aliasing errors, paper presented at Gravity, Geoid and Space Mission, Univ. of Porto, Porto, Portugal.

Swenson, S., and J. Wahr (2002), Methods for inferring regional surface-mass anomalies from Gravity Recovery and Climate Experiment (GRACE) measurements of time-variable gravity, *J. Geophys. Res.*, *107*(B9), 2193, doi:10.1029/2001JB000576.

Swenson, S., J. Wahr, and P. C. D. Milly (2003), Estimated accuracies of regional water storage variations inferred from the Gravity Recovery and Climate Experiment (GRACE), *Water Resour. Res.*, *39*(8), 1223, doi:10.1029/2002WR001808.

Tapley, B. D., S. Bettadpur, J. C. Ries, P. F. Thompson, and M. M. Watkins (2004), GRACE measurements of mass variability in the Earth system, *Science*, *23*(305), 503–505.

Wahr, J., M. Molenarr, and F. Bryan (1998), Time variability of the Earth's gravity field: Hydrological and oceanic effects and their possible detection using GRACE, *J. Geophys. Res.*, *103*(B12), 30,205–30,229.

Wahr, J., S. Swenson, V. Zlotnicki, and I. Velicogna (2004), Time-variable gravity from GRACE: First results, *Geophys. Res. Lett.*, *31*, L11501, doi:10.1029/2004GL019779.

J. L. Chen, Center for Space Research, University of Texas at Austin, Austin, TX 78712, USA. (chen@csr.utexas.edu)

J. S. Famiglietti, Department of Earth System Science, University of California, Irvine, CA 92697, USA. (jfamigli@uci.edu)

M. Rodell, NASA Goddard Space Flight Center, Greenbelt, MD 20771, USA. (matthew.rodell@nasa.gov)

K.-W. Seo, Jet Propulsion Laboratory, MS 183-501, California Institute of Technology, 4800 Oak Grove Drive, Pasadena, CA 91109, USA. (kiweon.seo@jpl.nasa.gov)

C. R. Wilson, Department of Geological Sciences, Jackson School of Geosciences, University of Texas at Austin, Austin, TX 78712, USA. (kiweon@geo.utexas.edu; crwilson@maestro.geo.utexas.edu)